

## $\ell_1$ SABMIS: $\ell_1$ -minimization and sparse approximation based blind multi-image steganography scheme

Rohit Agrawal

*Data & Computational Sciences Laboratory, Indian Institute of Technology Indore,  
Indore, 453552, India  
phd1501201004@iiti.ac.in*

Steganography plays a vital role in achieving secret data security by embedding it into cover media. The cover media and the secret data can be text or multimedia, such as images, videos, etc. In this paper, we propose a novel  $\ell_1$ -minimization and sparse approximation based blind multi-image steganography scheme, termed  $\ell_1$ SABMIS. By using  $\ell_1$ SABMIS, multiple secret images can be hidden in a single cover image. In  $\ell_1$ SABMIS, we sampled cover image into four sub-images, sparsify each sub-image block-wise, and then obtain linear measurements. Next, we obtain DCT (Discrete Cosine Transform) coefficients of the secret images and then embed them into the cover image's linear measurements.

We perform experiments on several standard gray-scale images, and evaluate embedding capacity, PSNR (peak signal-to-noise ratio) value, mean SSIM (structural similarity) index, NCC (normalized cross-correlation) coefficient, NAE (normalized absolute error), and entropy. The value of these assessment metrics indicates that  $\ell_1$ SABMIS outperforms similar existing steganography schemes. That is, we successfully hide more than two secret images in a single cover image without degrading the cover image significantly. Also, the extracted secret images preserve good visual quality, and  $\ell_1$ SABMIS is resistant to steganographic attack.

Keywords: Image Processing; Steganography; Sparse Approximation; Optimization;  $\ell_1$ -Minimization.

### 1. Introduction

The security of digital data is essential for its transfer over the communication media. To achieve this data security, in general, there are mainly two approaches used; cryptography<sup>30</sup> and steganography.<sup>24</sup> In cryptography, the encryption mechanism transforms plain-text (i.e., secret data) into cipher-text using the encryption key. This cipher-text appeared as an unreadable form that attracts opponents to manipulate its contents by using certain brute-force attacks.<sup>30</sup> Nevertheless, steganography avoids this situation.

Steganography is derived from two Greek words; steganos means “covered or secret,” and graphie means “writing”. The purpose of steganography is to hide the secret data into some other unsuspected cover media so that the secret data becomes visually imperceptible. In steganography, both the cover media and the secret data can be text or multimedia. The media obtained after embedding secret data into cover media is called stego-media. In this paper, we consider both the secret

2 *Rohit Agrawal*

data and the cover media as images due to their heavy use in web-based applications. The challenges here are: enhancing the embedding capacity, preserving the quality of the stego-image, and the scheme should be resistant to steganalysis<sup>a</sup> (i.e., steganographic attacks). In the following paragraphs, first, we discuss different categories of steganography schemes. Second, we discuss some of the existing schemes and their weaknesses. Finally, we discuss how the scheme proposed in this paper outperforms the existing schemes.

In general, image steganography can be categorized based on the domain in which embedding is performed, i.e., the spatial domain or the transformation domain. In the spatial domain-based scheme, secret data is embedded directly into the cover image by some alteration in image pixels value.<sup>8,11,19,28,34</sup> In the transform domain-based scheme, initially, the cover image is transformed into frequency components by certain transformations, and then the secret data is embedded into these components. A few of those schemes are JSteg,<sup>17</sup> F5,<sup>35</sup> Outguess,<sup>27</sup> etc.<sup>7,18,21,24,25</sup> The steganography scheme can also be categorized based on their embedding mechanisms, i.e., direct embedding or indirect embedding. In a direct embedding mechanism, the secret data is embedded by flipping the LSB (Least Significant Bit) of either the pixel value (i.e., spatial domain-based schemes) or the transformed coefficients (i.e., transform domain-based schemes) of the cover image.<sup>7,11,17,27</sup> In an indirect embedding mechanism, the pixel value or the transformed coefficient values are altered according to certain secret message bits.<sup>21,24,25,35</sup>

The spatial domain-based image steganography schemes outperform the transform domain one in-terms of embedding capacity. But they are not resistant to steganographic attack. Transform-based schemes are resistant to these attacks and provide good visual quality stego-image with limited embedding capacity. Furthermore, if we try to increase the embedding capacity of these schemes, then the quality of stego-image degrades. Besides, the indirect embedding mechanisms make steganography schemes more resistant to these attacks<sup>12,23,26,36,39</sup> as compared to direct ones. Thus, some of the schemes mentioned above are not resistant to steganographic attack.<sup>7,17,27</sup> While some are resistant to these attacks.<sup>21,24,25,35</sup>

The purpose of the scheme proposed in this paper is to hide multiple secret images in a single cover image. Hence, first, we discuss some recent image steganography schemes that hide multiple secret images in a single cover image. In,<sup>16</sup> the authors proposed a steganography scheme in which they hide two gray-scale secret images in a single color image. This scheme is based on two-level DWT (Discrete Wavelet Transformation). In this, the quality of stego-image and extracted images are good, but the embedding capacity in bit per pixel is very less. In,<sup>14</sup> the authors proposed a steganography scheme in which they hide three binary secret images in a single gray-scale as well as in a color image. This scheme is based on LSB based embedding approach, which is not resistant to steganographic attack. In this, the quality of stego-image is good, but the embedding capacity in bit per pixel is very

<sup>a</sup>It is the study of detecting the secret data hidden using steganography.

less.

Now, we discuss some recent image steganography schemes that hide only one secret image in a single cover image. In,<sup>29</sup> a gray-scale secret image is embedded in a color image. This scheme is based on DWT and PSO (particle swarm optimization). In,<sup>4</sup> a binary medical image is embedded in to a gray-scale cover image. This scheme is based on Redundancy Integer Wavelet Transform (RIWT), SVD (Singular Value Decomposition), and Discrete Cosine Transformation (DCT). In,<sup>3</sup> a binary medical image is embedded in a color cover image. This scheme is based on RIWT, DCT, and QR factorization. In all these schemes, the stego-image preserved good visual quality, but their embedding capacity is limited. And, if we try to increase this embedding capacity, the quality of the stego-image degrades.

To overcome this limitation, in this manuscript, we utilize other paradigms; optimization (i.e.,  $\ell_1$ -minimization) and sparse approximation. The steganography scheme proposed in this manuscript is termed as  $\ell_1$ SABMIS because we use the concept of  $\ell_1$ -minimization and sparse-approximation for blind multi-image steganography scheme.  $\ell_1$ SABMIS fulfills all the requirements of image steganography, i.e., it has high embedding capacity, preserve good visual quality stego-image, and resistant to steganographic attacks. Here, first, the cover image is sampled into four sub-images. Next, each sub-image is sparsified using DCT, and then its linear measurements are obtained using a random measurement matrix. Next, we collect the DCT coefficients of all secret images. Now, we select fix number of these coefficients for each secret image and then embed them into the permissible linear measurements using our proposed embedding rule (discussed in Section 3) and obtain modified measurements. Finally, we generate the stego-image from these modified measurements by solving the  $\ell_1$ -minimization problem (again, discussed in Section 3).

In  $\ell_1$ SABMIS, as discussed earlier, we embed DCT coefficients of secret images into linear measurements of the cover image, instead of embedding them directly into the transformed coefficients. These measurements act as encoded transformed coefficients, and hence, also adds security to our proposed scheme. For performance evaluation, we perform experiments on standard test images and evaluate embedding capacity, PSNR (Peak Signal-to-Noise Ratio) value,<sup>24</sup> mean SSIM (Structural Similarity) index,<sup>33</sup> NCC (Normalized Cross-Correlation) coefficient,<sup>20</sup> NAE (Normalized Absolute Error, also called normalized average absolute difference),<sup>20</sup> and entropy.<sup>13</sup> We also show the visual comparison between the cover image & its corresponding stego-image, and between the secret image & its corresponding extracted secret image. Moreover, we also show that our scheme outperforms existing image steganography schemes.

The rest of the paper is organized as follows. Section 2 gives brief explanation of each of  $\ell_1$ -minimization and sparse approximations. Section 3 explains our proposed steganography scheme, including embedding and extraction of the secret image. Section 4 presents experimental results. Finally, Section 5 gives conclusions and future work.

4 Rohit Agrawal

## 2. Background

Here, in the following subsections, we provide a brief explanation of  $\ell_1$ -minimization and sparse approximation.

### 2.1. $\ell_1$ -Minimization

The general form of the  $\ell_1$ -minimization is given as<sup>1,5</sup>

$$\begin{aligned} \min_x \|x\|_1 \\ \text{Subject to } Ax = b, \end{aligned} \quad (2.1)$$

where  $\|\cdot\|_1$  is the  $\ell_1$ -norm,  $x \in R^{N \times 1}$ ,  $A \in R^{M \times N}$ , and  $b \in R^{M \times 1}$ . In many applications such as signal processing, pattern recognition, etc., a  $\ell_1$ -minimization or a minimum  $\ell_1$ -norm solution is preferable. A few examples of these applications include data separation, face recognition, data clustering, image restoration, image classification, etc.

### 2.2. Sparse Approximation

Many practical problems in digital image processing and other disciplines include finding the best approximate solution to a system of linear equations. The theory of sparse approximation corresponds with sparse solutions for linear equation systems. This theory has applications in many domains, such as signal/ image processing, machine learning, medical imaging, etc.

Let, we have an unknown  $K$ -sparse signal  $x \in R^{N \times 1}$ , a measurement matrix  $\Phi \in R^{M \times N}$ , and a measurement vector  $y \in R^{M \times 1}$ , such that  $y = \Phi x$ . Reconstruction (or approximate reconstruction) of  $x$  from  $\Phi$  and  $y$ , which is usually considered as an inverse problem, can be obtained by solving the following  $\ell_0$ -minimization problem:<sup>2</sup>

$$\begin{aligned} \min_x \|x\|_0 \\ \text{Subject to } \Phi x = y, \end{aligned} \quad (2.2)$$

where  $\|\cdot\|_0$  is  $\ell_0$ -norm, which measures the total number of non-zero elements in a vector. This equation (i.e., (2.2)) is referred to as  $\ell_0$ -norm minimization problem,<sup>2</sup> which is a combinatorial and NP-hard problem.<sup>15</sup> Since the solution of  $x$  is sufficiently sparse, we can substitute the  $\ell_0$ -norm minimization by the  $\ell_1$ -norm (i.e., the closest convex norm) minimization problem. Hence,  $x$  is reconstructed from  $\Phi$  and  $y$  by the solving (2.1), where  $A$  and  $b$  are equivalent to  $\Phi$  and  $y$ , respectively.

As discussed, the signal to be approximated (or reconstructed) should be sparse. However, there are cases when this signal is not sparse. So, we can sparsify it using some transformation. For example, the signal  $x$ , which is not sparse, can be *sparsified* using an orthogonal matrix (termed as sparsification matrix)  $\Psi \in R^{N \times N}$  as

$$s = \Psi^T x, \quad (2.3)$$

where  $s \in R^{N \times 1}$  is the sparse representation of  $x$ . Sparse signal  $s$  can be reconstructed by solving (2.1), where the decision variable  $x$  is equivalent to  $s$ ,  $A$  is equivalent to  $\Theta = \Phi\Psi$ , and  $b$  is equivalent to  $y$ . After that, signal  $x$  is obtained from  $s$  by inverse *sparsification*, i.e.,  $x = \Psi s$ .

The approach of reconstructing sparse signal by solving (2.1) is referred as a convex optimization method. Some other approaches such as LASSO,<sup>6,32</sup> OMP,<sup>9</sup> CoSaMP,<sup>22</sup> SpaRSA,<sup>38</sup> etc.<sup>37</sup> can be used to reconstruct the sparse signal from the measurements.

### 3. Proposed Blind Multi-Image Steganography Scheme

Our proposed blind multi-image steganography scheme, which is based on  $\ell_1$ -minimization and sparse approximation, consists of embedding secret images and their extraction from the generated stego-image. These parts are discussed in the respective subsections below.

#### 3.1. Secret Images Embedding

First, we perform sub-sampling on a cover image and obtain four sub-sampled images (or sub-images). Let  $CI$  is the cover image of size  $N \times N$ , then the four sub-images are obtain as

$$\begin{aligned} CI^1(n_1, n_2) &= CI(2n_1 - 1, 2n_2 - 1), \\ CI^2(n_1, n_2) &= CI(2n_1, 2n_2 - 1), \\ CI^3(n_1, n_2) &= CI(2n_1 - 1, 2n_2), \\ CI^4(n_1, n_2) &= CI(2n_1, 2n_2), \end{aligned} \quad (3.1)$$

where  $n_1, n_2 = 1, 2, \dots, \frac{N}{2}$  (in our case,  $N$  is completely divisible by 2);  $CI^k$ , for  $k = \{1, 2, 3, 4\}$ , are the four sub-images; and  $CI(\cdot, \cdot)$  is the pixel value at  $(\cdot, \cdot)$ .

Originally, these sub-images are not sparse; hence, next, we perform block-wise sparsification of each of these images. For this, we divide each sub-image into blocks of size  $b \times b$  and obtain  $\frac{N^2}{4 \times b^2}$  blocks for each sub-image (in our case,  $b$  completely divides  $N$ ). Now, we consider each block as a vector of size  $b^2 \times 1$ , and then sparsify them (as in (2.3)) using discrete cosine transform matrix of size  $b^2 \times b^2$  as the sparsification matrix  $\Psi$ . That is,

$$s_i = \Psi^T x_i, \quad (3.2)$$

where  $i = 1, 2, \dots, \frac{N^2}{4 \times b^2}$ ,  $x_i$  and  $s_i$  are the  $i^{th}$  original and sparse vector representation of the respective blocks, and  $\Psi^T$  is the transpose of  $\Psi$ . Now, we consider these sparse vector in the zig-zag scanning order as given in one of our previous paper.<sup>24</sup> As a consequence of sparsification, each sparse vector has few coefficients of significant values and the remaining coefficients of very small or zero values. Thus, we categories each vector into two groups  $s_{i,u} \in R^{p_1}$  and  $s_{i,v} \in R^{p_2}$ , where  $p_1$  and  $p_2$  are the number of coefficients having large values and small values (or

6 Rohit Agrawal

zero values), respectively, and  $p_1 + p_2 = b^2$ . Now, we project each sparse vector onto linear measurements as

$$y_i = \begin{bmatrix} y_{i,u} \\ y_{i,v} \end{bmatrix} = \begin{bmatrix} s_{i,u} \\ \Phi s_{i,v} \end{bmatrix}, \quad (3.3)$$

where  $\Phi$  is the measurement matrices, which is a  $m \times p_2$  (for our case,  $m > p_2$ ) matrix of normally distributed random numbers; and  $y_i \in R^{(p_1+m) \times 1}$  is the set of linear measurements. Since the distribution of coefficients of the generated sparse vectors is almost the same for all blocks of an image, we use the same measurement matrix for all blocks.

Next, we perform processing in the secret images for embedding them into the cover image. In our proposed steganography scheme, we can embed a maximum of four secret images, one in each of the four sub-images of a single cover image. If we want to embed less than four secret images, we randomly select numbers of sub-images equal to the number of secret images that we want to embed, from the total four sub-images. Let  $S^k$ , for  $k = \{1, 2, 3, 4\}$ , are the four secret images each of the size  $M \times M$ . First, we perform block-wise DCT to each of these images and obtain their corresponding DCT coefficients. Here, the size of each block is  $l \times l$ , and hence, we have  $\frac{M^2}{l^2}$  number of blocks for each secret image (in our case,  $l$  completely divides  $M$ ). Now, we consider these DCT coefficients as a vector in the zig-zag scanning order as given in.<sup>24</sup> Let  $t_i^k \in R^{l^2 \times 1}$ , for  $i = 1, 2, \dots, \frac{M^2}{l^2}$ , be the vector representation of the DCT coefficients of the  $S^k$  secret image.

Now, we perform embedding of the secret images in the cover image. We embed  $t_i$  DCT coefficients from the secret image into  $y_i$  linear measurements of one sub-image of the cover image. This embedding is given in **Algorithm 1** that proposes the embedding rule. In this, we show embedding of only one secret image into one sub-image.

In this algorithm,  $p_1$  represents the number of coefficients having large values (as discussed above),  $p_3$  is the number of DCT coefficients from each  $t_i$  that are embedded into the cover sub-image, and  $\alpha$ ,  $\beta$ ,  $\gamma$  &  $c$  are the constants. Here, the steps number 2, 3 and 5 shows the embedding of the first coefficient, the next  $c - 1$  coefficients, and the remaining coefficients, respectively. Note that here, we choose all the parameters such that  $\frac{M^2}{l^2}$  will be less than or equal to  $\frac{N^2}{4 \times b^2}$ ,  $p_3$  coefficient from  $t_i$  can be embedded into  $y_i \in R^{p_1+m} \times 1$  using **Algorithm 1**, and the stego-images & the extracted secret images preserve good visual quality. We discuss the values of all these parameters in Experimental Results section (i.e., in section 4).

Finally, we construct the stego-image. As earlier, we can embed a maximum of four secret images into four sub-images of a single cover image. Hence, we first construct four sub-stego-images and then perform inverse sampling to obtain a stego-image from these four sub-stego-images. Let  $s'_i$  be the sparse vector of the  $i^{th}$

---

**Algorithm 1** Embedding Rule

---

**Input:**

- $y$ : Sequence of linear measurements of the cover image.
- $t$ : Sequence of transform coefficients of the secret image.
- The value of  $p_1$ ,  $p_3$ ,  $\alpha$ ,  $\beta$ ,  $\gamma$  and  $c$  (discuss in Sections 3.1 and 4).

**Output:**

- $y'$ : The modified version of the linear measurements.

1: Initialize  $y'$  to  $y$   
 2: **for**  $i = 1$  to  $\frac{N^2}{4 \times b^2}$  **do**

$$y'_i(p_1) = y_i(p_1 - 2c) + \alpha \times t_i(1).$$

3:   **for**  $j = p_1 - c + 1$  to  $p_1 - 1$  **do**

$$y'_i(j) = y_i(j - c) + \beta \times t_i(j - p_1 + c + 1).$$

4:   **end for**

5:   **for**  $k = p_1 + p_3 + 1$  to  $p_1 + 2 \times p_3 - c$  **do**

$$y'_i(k) = y_i(k - p_3 + c) + \gamma \times t_i(k - p_1 - p_3 + c).$$

6:   **end for**

7: **end for**

8: **return**  $y'$ 

---

block of a sub-stego-image (say  $k^{th}$ ), then

$$\begin{aligned} s'_{i,u} &= y'_i(1 : p_1) \text{ and} \\ s'_{i,v} &= \min_{s'_{i,v}} \|s'_{i,v}\|_1 \end{aligned} \quad (3.4)$$

$$\text{Subject to } \Phi s'_{i,v} = y'_i(p_1 + 1 : p_1 + m).$$

where  $y'_i(a : b)$  is the range from  $a^{th}$  element to  $b^{th}$  element of the vector  $y'_i$ . For the solution of the minimization problem of (3.4), we use LASSO (least absolute shrinkage and selection operator) formulation of it and then solve it using ADMM (alternating direction method of multipliers) algorithm.<sup>6,32</sup> The reason for this is that it has a wide application in the image processing domain. The sparse vector  $s'_i$  is the concatenation of  $s'_{i,u}$  and  $s'_{i,v}$ . After that, we perform inverse sparsification and obtain non-sparse vectors as  $x'_i = \Psi s'_i$ . Now, we covert each vector  $x'_i$  into block of size  $b \times b$ , and then construct the sub-stego-image of size  $\frac{N}{2} \times \frac{N}{2}$  by arranging all these blocks. In the end, we perform inverse sampling (see (3.1)) and obtain a single stego-image from the four sub-stego-images.

### 3.2. Secret Images Extraction

In this subsection, we discuss the process of extraction of the secret images from the stego-image. Initially, we perform sampling (as done in subsection 3.1 using (3.1)) onto the stego-image to obtain four sub-stego-images. Let  $T^k$ , for  $k = \{1, 2, 3, 4\}$ , are the four sub-stego-images. Since the extraction of all the secret images is similar, here, we discuss the extraction of only one secret image from one sub-stego-image. In this process, first, we perform block-wise sparsification of the sub-stego-image. For this, we divide this image into blocks of size  $b \times b$  and then consider each block as a vector of  $b^2 \times 1$ . Here, we have a total of  $\frac{N^2}{4 \times b^2}$  blocks for a sub-stego-image. Next, we sparsified each vector (say  $x_i''$ ), as done in subsection 3.1, using the same sparsification matrix and (3.2), and then obtain sparse vector (say  $s_i''$ ).

Next, as earlier, we consider these sparse vector in the zig-zag scanning order, and then categories each vector into two groups  $s_{i,u}'' \in R^{p_1}$  and  $s_{i,v}'' \in R^{p_2}$ , where as earlier,  $p_1$  and  $p_2$  are the number of coefficients having large values and small values (or zero values), respectively. After that, we project each sparse vector onto linear measurements (say  $y_i'' \in R^{(p_1+m) \times 1}$ ), as done in subsection 3.1, using the same measurement matrix  $\Phi \in R^{m \times p_2}$  and (3.3). This  $y_i''$  have DCT coefficients of the secret image that is extracted by the extraction rule given in **Algorithm 2**. This extraction rule is reverse of the embedding rule, given in **Algorithm 1**.

In **Algorithm 2**, the size of  $t_i'$  is same as the size of  $t_i$ , i.e.,  $l^2 \times 1$ . After extracting DCT coefficients  $t'$  from the stego-image, we convert each vector  $t_i'$  into the blocks of size  $l \times l$ , and then perform block-wise inverse discrete cosine transformation (IDCT) to obtain secret image pixels. Finally, we obtain extracted secret image of size  $M \times M$  by arranging all these blocks.

As mentioned earlier, this steganography scheme is a blind multi-image steganography scheme because it does not require any cover image data at the receiver side for the extraction of secret images.

## 4. Experimental Results

Experiments are carried out in *MATLAB* on a machine with Intel Core i3 processor @2.30 GHz and 4GB RAM. We use a set of standard gray-scale images to test our  $\ell_1$ SABMIS. Some sample test images used in our experiments are shown in Fig. 1. These images are taken from the USC-SIPI image database,<sup>31</sup> and have varying texture property. In this paper, we take all these ten images as the cover images, and four images (Fig. 1a, Fig. 1b, Fig. 1e and Fig. 1j) as the secret images for our experiments. However, we can use any of the ten images apart from these four as the secret image.

Though the images shown in Fig. 1 seems to be of same size, however for our experiments, the size of each cover image is kept as  $1024 \times 1024$  (i.e.,  $N \times N$ ), and the size of each secret image is kept as  $512 \times 512$  (i.e.,  $M \times M$ ). We take blocks of size  $8 \times 8$  for both the cover images and the secret images (i.e.,  $b \times b$  and  $l \times l$ ). Recall from subsection 3.1, the size of measurement matrix  $\Phi$  is  $m \times p_2$ ,

**Algorithm 2** Extraction Rule**Input:**

- $y''$ : Sequence of linear measurements of the stego-image.
- The value of  $p_1, p_3, \alpha, \beta, \gamma$  and  $c$  (discuss in Sections 3.1 and 4).

**Output:**

- $t'$ : Sequence of transform coefficients of the extracted secret image.

- 1: Initialize  $t'$  to zeros
- 2: **for**  $i = 1$  to  $\frac{N^2}{4 \times b^2}$  **do**

$$t'_i(1) = \frac{y''_i(p_1) - y''_i(p_1 - 2c)}{\alpha}.$$

- 3:     **for**  $j = p_1 - c + 1$  to  $p_1 - 1$  **do**

$$t'(j - p_1 + c + 1) = \frac{y''_i(j) - y''_i(j - c)}{\beta}.$$

- 4:     **end for**

- 5:     **for**  $k = p_1 + p_3 + 1$  to  $p_1 + 2 \times p_3 - c$  **do**

$$t'(k - p_1 - p_3 + c) = \frac{y''_i(k) - y''_i(k - p_3 + c)}{\gamma}.$$

- 6:     **end for**

- 7: **end for**

- 8: **return**  $t'$

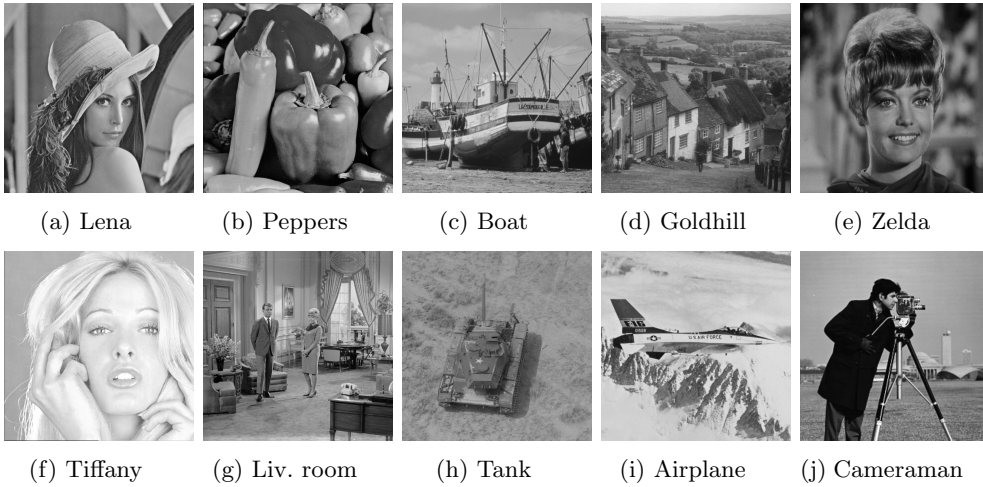


Fig. 1: Test images used in our experiments

where  $p_1 + p_2 = b^2$  (here,  $b^2 = 64$ ). Usually, for most images, more than half of the coefficient in a DCT sparsified vector has value either very small or zero. Hence, in our experiments, we take  $p_1 = p_2 = 32$ , and  $m = 10 \times p_2$  (i.e, we over-sampled linear measurements). In general, the DCT coefficients can be divided into three sets, low frequencies, middle frequencies, and high frequencies. Low frequencies are associated with the illumination, middle frequencies are associated with the structure, and high frequencies are associated with the noise or small variation details. We discarded these high-frequency coefficients, which are usually half of the total coefficients. Hence, we take  $p_3 = 32$ . Due to the property of DCT, the first coefficient have the highest value, then a few coefficients have values lower than the first one, and remaining coefficients have values lowest. These three category of coefficients are embedded in the step numbers 2, 3 and 5 of **Algorithm 1**, respectively. Hence, to obtain good quality extracted secret image, we take  $\alpha = 0.01$ ,  $\beta = 0.1$ ,  $\gamma = 1$ , and  $c = \{6, 8\}$  (the results are reported for only one value of  $c$  that gave better performance).

A successful steganography scheme should have high embedding capacity, and should not distort the cover media significantly (i.e., the distortion should be visually imperceptible). Thus, we evaluate the performance of our proposed  $\ell_1$ SABMIS by analyzing these two metrics. As this paper proposes a multi-image steganography scheme, we evaluate the performance of  $\ell_1$ SABMIS for the cases where all the four images and less than four images are embedded.

The embedding capacity (or embedding rate) is the number (or length) of secret information bits that can be embedded in each pixel of the cover image. It is measured in bits per pixel (bpp). Thus, we have embedding capacities of 2 bpp, 4 bpp, 6 bpp, and 8 bpp for embedding one, two, three, and four secret images, respectively. Next, we evaluate the quality of the stego-image. Imperceptibility is the measure of the invisibility of the secret image that is hidden in the generated stego-image. There is no universal criterion to determine imperceptibility. However, we evaluate it by visual and numerical (PSNR, MSSIM, NCC, NAE, and Entropy) metrics.

We construct stego-images corresponding to different test images used in our experiments and then check the distortion visually. We also check their corresponding edge map diagrams. Here, we present the visual comparison only for ‘Zelda’ cover image. This comparison is given in Fig. 2. In this figure, 2a shows ‘Zelda’ cover image, 2b shows stego-image, 2c shows the edge map diagram of cover image, and 2d shows the edge map diagram of stego-image. From these sub-figures, we observe that the stego-image is almost similar to its corresponding cover image. Also, their corresponding edge maps are almost the same.

The numerical metrics evaluate imperceptibility by comparing the cover images and their corresponding stego-images based on some numerical criteria. These include; PSNR value, mean SSIM index, NNC coefficient, NAE, and entropy. PSNR<sup>10</sup> value is evaluated in decibel (dB), and its higher value indicates the higher imperceptibility of the stego-image. In general, value above 30 dB is considered to be good

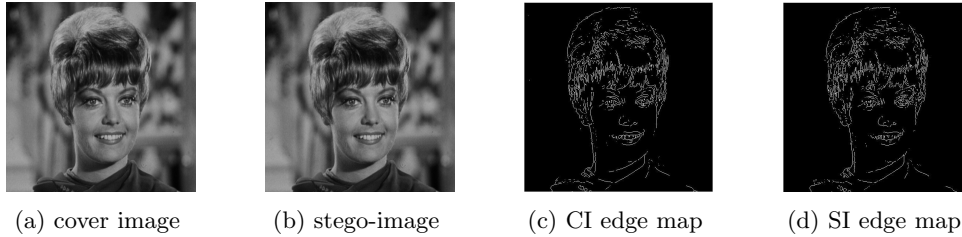


Fig. 2: Visual quality analysis between ‘Zelda’ cover image (CI) and its corresponding stego-image (SI)

for the quality of the stego-image.<sup>21,40</sup> For more details, please see.<sup>24</sup> The PSNR values of the stego-images corresponding to different test images are given in Fig. 3 and Fig. 4. In Fig. 3, we show the PSNR values for the four cases, i.e., embedding one, two, three, and four images. As we have four secret images, we have the choice of embedding any one of them and present its corresponding PSNR value. However, we embed all four images individually, obtain their PSNR values, and then present the average of these four PSNR values. Similarly, the average PSNR values are presented for the cases when we embed two and three images. For the case of embedding four images, there is only one choice, and hence its corresponding PSNR value is presented.

In Fig. 4, we show the PSNR values of all the stego-images when all the four secret images are embedded separately. In this figure, we observe the highest PSNR value (i.e., 47.32 dB) when ‘Zelda’ secret image is hidden in ‘Zelda’ cover image, while the lowest PSNR value (i.e., 40.21 dB) when ‘Peppers’ secret image is hidden in ‘Boat’ cover image. Also, we observe that for all the cases, we obtain PSNR values higher than 30 dB, and hence, considered good.

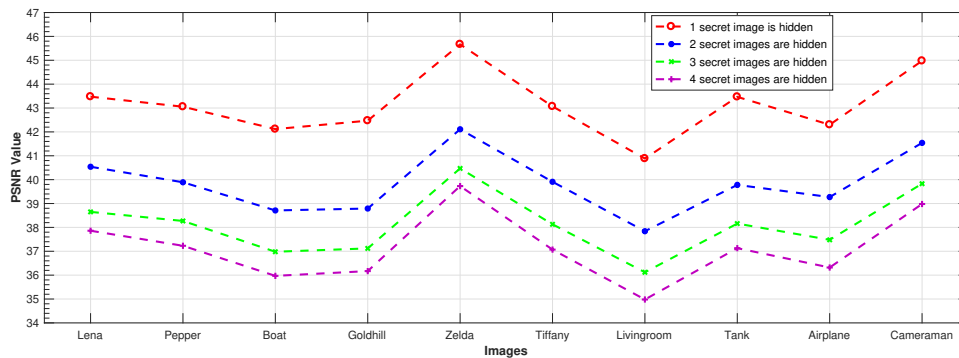


Fig. 3: PSNR value of the stego-images when different number of images are hidden

12 Rohit Agrawal

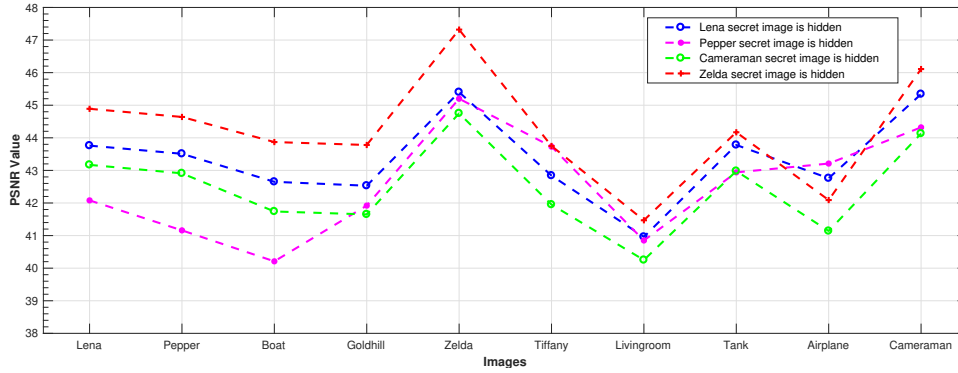


Fig. 4: PSNR value of the stego-images when only 1 secret image is hidden

We measure the structural similarity between the cover images and their corresponding stego-images by the metric of mean SSIM.<sup>33</sup> The value of mean SSIM index lies between 0 and 1, where the value 0 implies that there is no similarity between the cover image and stego-image, and the value 1 implies that the cover image is exactly similar to its corresponding stego-image. We measure the degree of similarity between the cover images and their corresponding stego-images by another metric called normalized cross-correlation (NCC) coefficients.<sup>20</sup> Similar to mean SSIM, the value of NCC equal to 1 implies that the cover image is exactly similar to its corresponding stego-image. We also measure the quality of stego-image by evaluating NAE<sup>20</sup> between the cover images and their corresponding stego-images. A value close to 0 indicates that the stego-image is almost similar to their corresponding cover image. Moreover, we also measure the entropy of the cover images and their corresponding stego-images. Entropy is a statistical randomness measure, which can be used to characterize the texture of an image.<sup>13</sup> In Table 1, we give the values of all these metrics for our  $\ell_1$ SABMIS when hiding all the four secret images. We do not present the values for the cases of embedding less than four secret images as their results will be better than those given in Table 1.

From this table, we observe that all the values of mean SSIM index are equal to 1. Hence, the cover images and their corresponding stego-images are similar in structure. The values of NCC coefficients are also close to 1. The values of NAE are close to 0. The values of entropy of stego-images are almost similar to their corresponding cover images. Thus, we can say that the stego-images and their corresponding cover images are almost identical. In addition to high embedding capacity with good quality stego-image,  $\ell_1$ SABMIS is also resistant against *steganographic* attacks. The reason for this is that  $\ell_1$ SABMIS is a transformed domain-based technique. And, in this scheme, we embed secret images by an indirect embedding strategy (i.e., LSB flipping based embedding is not adopted).

Table 1: Mean SSIM (MSSIM) index, NCC coefficient, NAE, and entropy of the stego-image.

Cover Image	MSSIM	NCC	NAE	Entropy	
				Original image	Stego-image
Lena	1	0.9992	0.009	7.443	7.463
Pepper	1	0.9997	0.012	7.573	7.598
Boat	1	0.9998	0.012	7.121	7.146
Goldhill	1	0.9998	0.013	7.471	7.486
Zelda	1	0.9964	0.011	7.263	7.272
Tiffany	1	0.9999	0.006	6.602	6.628
Livingroom	1	0.9996	0.013	7.431	7.438
Tank	1	0.9998	0.014	6.372	6.405
Airplane	1	0.9972	0.015	6.714	6.786
Cameraman	1	1.0000	0.009	7.055	7.123
<b>Average</b>	<b>1</b>	<b>0.9991</b>	<b>0.011</b>	<b>7.104</b>	<b>7.1343</b>

#### 4.1. Performance Comparison

In this subsection, we compare the performance of our  $\ell_1$ SABMIS with the existing steganography schemes. These results are given in Table 2.

Table 2: Performance comparison of our  $\ell_1$ SABMIS with various other steganography schemes.

Steganography Scheme	Embedding Capacity (in bpp)	PSNR (in dB)	Resistant to Steganographic Attacks?
16	1.33	44.75	Yes
14	2	46.36	No
29	2.67	48.25	Yes
4	0.5	51.15	Yes
3	0.25	49.69	Yes
<b>Hide 1 Image</b>	<b>2</b>	<b>44.98</b>	
<b>Hide 2 Images</b>	<b>4</b>	<b>42.54</b>	<b>Yes</b>
<b>Hide 3 Images</b>	<b>6</b>	<b>39.83</b>	
<b>Hide 4 Images</b>	<b>8</b>	<b>38.98</b>	

In this table, the first column represents various steganography schemes, and the remaining columns represent the metrics used for the comparison. As earlier, a successful steganography scheme should have high embedding capacity with a considerably good quality stego-image. Also, it should be resistant to steganographic attacks. Hence, we use embedding capacity, PSNR value, and checking which schemes are resistant to steganographic attacks or not as the performance metrics for the comparison. In this table, the embedding capacity is represented in bit per pixel,

where each pixel is considered as a gray-scale. For these existing schemes, the data is not available for all the test images used in this experiment. Hence, in this table, we report the average PSNR values of all the images given in the respective papers.

From this table, we observe that except<sup>14</sup> and,<sup>29</sup> our  $\ell_1$ SABMIS outperforms all other existing steganography schemes. The scheme proposed in<sup>14</sup> is based on LSB based embedding, which is not resistant to steganographic attacks. The scheme proposed in<sup>29</sup> embeds single secret image in a color image, which is different from our goal. Also, it has limited embedding capacity. Hence, we can say that out of all these schemes,  $\ell_1$ SABMIS embeds multiple secret images with high embedding capacity and good quality stego-image. Also,  $\ell_1$ SABMIS is resistant to steganographic attacks.

As discussed earlier, we also calculate the mean SSIM index, NCC coefficients, NAE, and entropy values for the performance evaluation. However, these results are not compared with other techniques because the data for the same are not available for these other techniques.

#### **4.2. Quality Assessment of Secret Recovered Image**

As earlier, PSNR value can be used to assess the quality of the secret recovered image, and the value greater than 30 dB is considered good. However, this is not true for every case. For example, the steganography scheme proposed in<sup>16</sup> has PSNR values greater than 30 dB for the extracted secret images. However, these images have black colored and white colored alternate horizontal and vertical lines. Hence, we only report other metrics to evaluate the quality of the extracted/ recovered secret image.

As human is the final spectator of the extracted secret image, human observers are considered the final arbiter to assess the quality of these images. In Fig. 5a and Fig. 5b, we show the ‘Pepper’ secret image and the extracted secret image from ‘Zelda’ stego-image. From these figures, we observe that there is very little distortion in the extracted image. Besides this, we also show their corresponding edge maps diagram in Fig. 5c and 5d, respectively. Again, we observe very little variation in their corresponding edge maps diagrams.

Moreover, we also evaluate the mean SSIM index, NCC coefficient, NAE, and entropy to measure the quality of the extracted secret images. The values of these metrics are given in Table 3. From this table, we observe that for all the images, the values of mean SSIM index is 1, NCC coefficient is close to 1, NAE is close to 0, and the entropy of the original secret images and their corresponding extracted secret images are almost the same. Thus, we see that the extracted secret image preserve good quality.

### **5. Conclusions and Future Work**

We present a blind multi-image steganography scheme based on  $\ell_1$ -minimization and sparse approximation. Here, we can embed a maximum of four secret im-

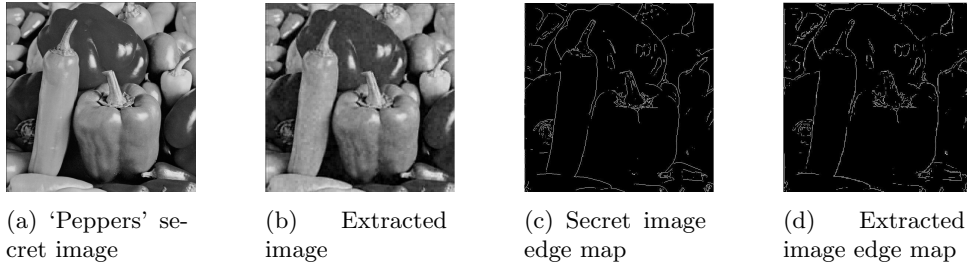


Fig. 5: Visual quality analysis between 'Peppers' secret image and 'Peppers' extracted image from 'Zelda' stego-image.

Table 3: Mean SSIM (MSSIM) index, NCC coefficient, NAE, and entropy of the extracted/ recovered secret image.

Secret Image	MSSIM	NCC	NAE	Entropy	
				Original Image	Recovered Image
Lena	1	0.9973	0.026	7.446	7.627
Pepper	1	0.9946	0.329	7.571	7.624
Camerman	1	0.9953	0.027	7.048	7.258
Zelda	1	0.9972	0.028	7.267	7.284
<b>Average</b>	<b>1</b>	<b>0.9961</b>	<b>0.103</b>	<b>7.333</b>	<b>7.449</b>

ages in a single cover image. Initially, we perform sampling in the cover image and obtain four sub-images. Next, we sparsify each sub-image and then obtain its linear measurements using a random measurement matrix. Finally, using our embedding rule, we embed DCT coefficients of the secret images into the linear measurements. The stego-image is obtained from the modified measurements by solving a  $\ell_1$ -minimization problem.

We perform experiments on several standard gray-scale images that vary in texture. For performance evaluation, we calculate embedding capacity, PSNR value, mean SSIM index, NCC coefficient, NAE, and entropy. Experiments show that our  $\ell_1$ SABMIS hides four secret images in a cover image without distorting it significantly and has PSNR values greater than 35 dB, which is usually considered good. Also, the mean SSIM index is equal to 1, the NCC coefficient is close to 1, and the value of NAE is close to 0, which shows that the stego-images are almost identical to its corresponding cover images. We obtain approximately the same entropy value for both the cover images and their corresponding stego-images. We also obtain almost same values for all the metrics (i.e., mean SSIM, NCC coefficients, NAE, and entropy) as above for the extracted secret images. This indicates that the extracted secret images preserve good visual quality. Finally,  $\ell_1$ SABMIS is also resistant to

steganographic attacks.

In the future, we plan to embed the secret images in other media such as audio, video, etc. We also plan to apply optimization techniques to calculate the values of parameters  $\alpha, \beta, \gamma$ , etc. used in our embedding and extraction algorithms.

## References

1. R. Agrawal, K. Ahuja, C. Hau Hoo, T. Duy Anh Nguyen and A. Kumar, ParaLarPD: Parallel FPGA router using primal-dual sub-gradient method, *Electronics* **8**(12) (2019) p. 1439.
2. R. A. M. Alsaidi and H. Li, Hierarchical sparse method with applications in vision and speech recognition, *International Journal of Wavelets, Multiresolution and Information Processing* **11**(2) (2013) p. 1350016.
3. S. Arunkumar, V. Subramaniaswamy, V. Vijayakumar, N. Chilamkurti and R. Logesh, SVD-based robust image steganographic scheme using RIWT and DCT for secure transmission of medical images, *Measurement* **139** (2019) 426–437.
4. S. Arunkumar, S. Vairavasundaram, K. Ravichandran and L. Ravi, RIWT and QR factorization based hybrid robust image steganography using block selection algorithm for IoT devices, *Journal of Intelligent & Fuzzy Systems* **35**(5) (2019) 4265–4276.
5. R. Ashino and R. Vaillancourt, Phase transitions in error correcting and compressed sensing by  $\ell_1$  linear programming, *International Journal of Wavelets, Multiresolution and Information Processing* **11**(4) (2013) p. 1360004.
6. S. Boyd, N. Parikh, E. Chu, B. Peleato and J. Eckstein, Distributed optimization and statistical learning via the alternating direction method of multipliers, *Found. Trends Mach. Learn.* **3** (Jan 2011) 1–122.
7. C.-C. Chang, T.-S. Chen and L.-Z. Chung, A steganographic method based upon jpeg and quantization table modification, *Information Sciences* **141**(1) (2002) 123 – 138.
8. Chi-Kwong Chan and L. M. Cheng, Improved hiding data in images by optimal moderately-significant-bit replacement, *Electronics Letters* **37** (Aug 2001) 1017–1018.
9. G. Davis, S. Mallat and M. Avellaneda, Adaptive greedy approximations, *Constructive approximation* **13**(1) (1997) 57–98.
10. Dejey and R. S. Rajesh, An improved wavelet domain digital watermarking for image protection, *International Journal of Wavelets, Multiresolution and Information Processing* **8**(1) (2010) 19–31.
11. S. Devi, M. N. Sahoo, K. Muhammad, W. Ding and S. Bakshi, Hiding medical information in brain MR images without affecting accuracy of classifying pathological brain, *Future Generation Computer Systems* **99** (2019) 235 – 246.
12. J. Fridrich, M. Goljan and D. Hoge, Steganalysis of JPEG images: Breaking the f5 algorithm, *Information Hiding*, ed. F. A. P. Petitcolas (Springer Berlin Heidelberg, Berlin, Heidelberg, 2003), pp. 310–323.
13. R. C. Gonzalez, R. E. Woods and S. L. Eddins, *Digital Image Processing Using MATLAB* (Prentice-Hall, Inc., Upper Saddle River, NJ, USA, 2003).
14. P. Guttikonda, H. Cherukuri and N. B. Mundukur, Hiding encrypted multiple secret images in a cover image, *Proceedings of International Conference on Computational Intelligence and Data Engineering*, (Springer, 2018), pp. 95–104.
15. Y. Haiying, S. Hongying, S. Xun, G. Kun and J. Zijian, Compressive sensing measurement matrix construction based on improved size compatible array ldpc code, *IET Image Processing* **9** (July 2015) 993–1001.
16. S. Hemalatha, U. D. Acharya, A. Renuka and P. R. Kamath, A secure image steganog-

- raphy technique to hide multiple secret images, *Computer Networks & Communications (NetCom)*, (Springer, 2013), pp. 613–620.
17. JSteg Source, <https://zooid.org/paul/crypto/jsteg/> accessed 3 March 2019.
  18. G. Kasana, K. Singh and S. S. Bhatia, EMD-based steganography techniques for JPEG2000 encoded images, *International Journal of Wavelets, Multiresolution and Information Processing* **15**(3) (2017) p. 1750020.
  19. M. Khodaei and K. Faez, New adaptive steganographic method using least-significant-bit substitution and pixel-value differencing, *IET Image processing* **6**(6) (2012) 677–686.
  20. M. Kutter and F. A. Petitcolas, Fair benchmark for image watermarking systems, *Security and Watermarking of Multimedia Contents*, **3657**, International Society for Optics and Photonics 1999, pp. 226–239.
  21. C.-L. Liu and S.-R. Liao, High-performance jpeg steganography using complementary embedding strategy, *Pattern Recognition* **41**(9) (2008) 2945 – 2955.
  22. D. Needell and J. Tropp, Cosamp: Iterative signal recovery from incomplete and inaccurate samples, *Applied and Computational Harmonic Analysis* **26**(3) (2009) 301 – 321.
  23. A. Nissar and A. Mir, Classification of steganalysis techniques: A study, *Digital Signal Processing* **20**(6) (2010) 1758 – 1770.
  24. A. K. Pal, K. Naik and R. Agrawal, A steganography scheme on jpeg compressed cover image with high embedding capacity, *Int. Arab J. Inf. Technol.* **16**(1) (2019) 116–124.
  25. J.-S. Pan, W. Li, C.-S. Yang and L.-J. Yan, Image steganography based on sub-sampling and compressive sensing, *Multimedia Tools and Applications* **74** (Nov 2015) 9191–9205.
  26. C. Patsakis, N. Aroukatos and S. Zimeras, Lsb steganographic detection using compressive sensing, *Intelligent Interactive Multimedia Systems and Services*, eds. G. A. Tsihrintzis, M. Virvou, L. C. Jain and R. J. Howlett (Springer Berlin Heidelberg, Berlin, Heidelberg, 2011), pp. 219–225.
  27. N. Provos, Defending against statistical steganalysis, *Proceedings of the 10th Conference on USENIX Security Symposium - Volume 10, SSYM'01*, (USENIX Association, Berkeley, CA, USA, 2001).
  28. S. Saeed and A. M. Ali, One-third probability embedding: a new  $\pm 1$  histogram compensating image least significant bit steganography scheme, *IET image processing* **8**(2) (2013) 78–89.
  29. M. Sanjutha, An image steganography using particle swarm optimization and transform domain, *International Journal of Engineering & Technology* **7**(224) (2018) 474–477.
  30. W. Stallings, *Cryptography and network security: principles and practice* (Pearson Upper Saddle River, 2017).
  31. The USC-SIPI Image Database, <http://sipi.usc.edu/database/> accessed 3 March 2019.
  32. R. Tibshirani, Regression shrinkage and selection via the lasso, *Journal of the Royal Statistical Society: Series B (Methodological)* **58**(1) (1996) 267–288.
  33. H. Wajihha, S. Tabinda, S. A. Masood and T. Imran, Wavelet denoising of multiframe optical coherence tomography data using similarity measures, *IET Image Processing* **11** (April 2016) 64–79.
  34. R.-Z. Wang, C.-F. Lin and J.-C. Lin, Image hiding by optimal lsb substitution and genetic algorithm, *Pattern Recognition* **34**(3) (2001) 671–683.
  35. A. Westfeld, F5—a steganographic algorithm, *Information Hiding*, ed. I. S. Moskowitz (Springer Berlin Heidelberg, Berlin, Heidelberg, 2001), pp. 289–302.

18 *Rohit Agrawal*

36. A. Westfeld and A. Pfitzmann, Attacks on steganographic systems, *Information Hiding*, ed. A. Pfitzmann (Springer Berlin Heidelberg, Berlin, Heidelberg, 2000), pp. 61–76.
37. D. P. Wipf and B. D. Rao, An empirical bayesian strategy for solving the simultaneous sparse approximation problem, *IEEE Transactions on Signal Processing* **55** (July 2007) 3704–3716.
38. S. J. Wright, R. D. Nowak and M. A. T. Figueiredo, Sparse reconstruction by separable approximation, *IEEE Transactions on Signal Processing* **57** (July 2009) 2479–2493.
39. T. Zhang and X. Ping, A fast and effective steganalytic technique against jsteg-like algorithms, *Proceedings of the 2003 ACM Symposium on Applied Computing, SAC '03*, (ACM, New York, NY, USA, 2003), pp. 307–311.
40. Y. Zhang, J. Jiang, Y. Zha, H. Zhang and S. Zhao, Research on embedding capacity and efficiency of information hiding based on digital images, *International Journal of Intelligence Science* **3**(02) (2013) p. 77.